Energy Balancing Improvement of Modular Multilevel Converters Under Unbalanced Grid Conditions

Andres E. Leon, *Senior Member, IEEE*, and Santiago J. Amodeo

***Abstract*—This paper presents a feedback/feed-forward control strategy to improve the voltage balancing of modular multilevel converters (MMCs) under unbalanced grid conditions. The inclusion of a feed-forward compensation improves the disturbance rejection capability against asymmetrical faults and sudden voltage imbalances in the ac grid. The floating capacitor voltages of the MMC are controlled in two stages. The first one equally distributes the voltages in each arm, and the second one balances the energy among the six arms. This last control stage is also divided into the called horizontal and vertical balancing. Based on a detailed analysis of the power terms disturbing the MMC arm energies, the control strategy is tailored to improve the voltage transient response by adding feed-forward terms to both horizontal and vertical balancing controls. In addition, various approaches to manage the MMC under unbalanced grid conditions are compared regarding several aspects, such as capacitor voltage ripple, balancing performance, and negative-sequence current injection. Advantages and disadvantages of both the proposed and the conventional energy-based control schemes are also studied, showing that the voltage control performance can be improved by enhancing the existing MMC control systems.**

***Index Terms*—Capacitor voltage balancing, feed-forward control, modular multilevel converter (MMC), unbalanced operation, voltage-source converter (VSC)-based high-voltage direct current (HVdc) transmission systems.**

I. Introduction

THE modular multilevel converter (MMC) is a promising technology for ac/dc power conversion in applications such as offshore wind farm integration, multiterminal dc grids, and flexible ac transmission systems [1]. The MMC can also be used in high-voltage direct current (HVdc) links, having the advantages of the voltage-source converters (VSCs) over the traditional line-commutated converters namely, independent control of active and reactive powers, fast transient response, capability to supply weak or passive networks, and black start capability [2].

The MMC was first proposed in 2002 [3] from a concept introduced by Alesina and Venturini [4] in 1981. Previously, the multilevel VSCs were mostly based on neutral-point-clamped (NPC), flying-capacitor (FC), and cascaded H-bridge (CHB) converters. These topologies present some drawbacks for high-power and high-voltage applications [5]. The NPC and FC converters have practical limitations due to the significant complexity increase when the number of levels is high; also, they do not have a fully modular and scalable design. The CHB converter has a modular structure, but the shortcoming of requiring isolated dc sources for its H-bridge modules. In comparison with these multilevel VSCs, the MMC has many advantages [6], among which are: 1) the higher modularity and scalability easily handles high voltages by cascade connection of hundreds of low-voltage submodules (SMs), thus avoiding long strings of series-connected insulated-gate bipolar transistors (IGBTs); 2) the higher number of voltage levels produces a nearly sinusoidal output waveform, allowing small (or no) harmonic filter requirements; 3) its lower switching frequency reduces the converter losses, reaching an efficiency closer to the thyristor technology. Other benefits of the MMC are that its hardware complexity grows linearly as the number of levels increases and its reliability is improved by using redundant SMs; it also has better fault management, smaller footprint, and it allows transformerless operation.

The MMC is currently being developed by many manufacturers such as Siemens, ABB, Alstom, and EPRI, representing the last generation of high-power VSCs. It has been implemented in the Trans Bay Cable project (a 400 MW HVdc link of $\pm$200 kV dc voltage and 216 SMs per arm), in the France-Spain electrical interconnection (INELFE) project (2×1000 MW HVdc links of $\pm$320 kV with 400 SMs), and in other projects in construction and planning stages [1].

The control system of the MMC controls the ac-side, dc-side, and circulating currents, but its most challenging task is to control and balance the floating capacitor voltages. For a proper operation, the MMC control strategy has to regulate the total energy stored in all the converter capacitors, to balance the energies among the arms (inter-arm balancing), and to equally distribute the voltages inside each arm (intra-arm balancing). The inter-arm balancing can be divided into horizontal balancing (inter-leg balancing) and vertical balancing (intra-leg balancing).

Manuscript received April 16, 2016; revised September 2, 2016; accepted October 21, 2016. Date of publication October 25, 2016; date of current version March 24, 2017. This work was supported in part by the Consejo Nacional de Investigaciones Científicas y Técnicas and in part by the Universidad Nacional del Sur, Argentina. Recommended for publication by Associate Editor Makoto Hagiwara.

A. E. Leon is with the Instituto de Investigaciones en Ingeniería Eléctrica "Alfredo Desages", Universidad Nacional del Sur, Bahía Blanca, Argentina (e-mail: aleon@iiie-conicet.gob.ar).

S. J. Amodeo is with the ElectroAMSA Company, Bahía Blanca, Argentina, and also with the Universidad Nacional del Sur, Bahía Blanca Argentina (e-mail: samodeo@uns.edu.ar).

Color versions of one or more of the figures in this paper are available online at http://ieeexplore.ieee.org.

Digital Object Identifier 10.1109/TPEL.2016.2621000

Several techniques have been proposed to control the SM capacitor voltages (see a description of the different techniques in [1] and [6]–[8]). They can be classified into distributed and centralized methods, open-loop and closed-loop schemes, and by those performing the voltage balancing before or after the modulation stage. For a particular application, the choice of the balancing technique depends on: the complexity when the number of levels increases, the impact on the switching frequency, the output waveform distortion, and the capacitor voltage ripple (see [9] and [10]). The sorting (or module selection) methods with reduced switching frequency (RSF) are very effective and widely used to perform the intra-arm balancing [7]. On the other hand, energy-based control schemes have recently gained attention to perform the inter-arm balancing because the arm energies can be controlled in a closed-loop manner, thus allowing to choose the convergence rate of the voltage balancing, and also because the balancing is achieved by acting on the internal circulating current so that the ac and dc output current waveforms are not affected [1].

The energy-based control scheme was introduced in [11], further developed in [12]–[15], and more recently studied in [16]–[19]. However, these works and other control approaches such as [20]–[23] considered balanced grid conditions when designing and testing the energy balancing controller. The MMC was analyzed under unbalanced ac grid conditions in [24]–[33], but these studies are only focused on the output and circulating current controls, and they do not discuss the inter-arm energy balancing issue. More recently, the energy-based control scheme was studied under unbalanced grid conditions in [34], but it was implemented with the same algorithm that the one previously proposed for balanced conditions. Modifications in the balancing algorithm were introduced in [35] and [36] to enhance the MMC operation during asymmetrical faults. These approaches have both advantages and disadvantages depending on the transient response performance, the requirement of an accurate grid phase tracking, as well as the amount of third-harmonic offset voltage and negative-sequence current injected by the balancing control [37].

In this work, improvements in the transient response and energy balancing performance of the MMC are achieved under grid imbalances and asymmetrical faults by adding feed-forward terms to both the horizontal and the vertical balancing controls. A detailed analysis of the power terms disturbing the MMC arm energies is presented and used to extend the energy-based control scheme to generalized grid voltage conditions. The inner current control loops are designed in a stationary reference frame and a discrete-time domain, which avoids tracking the phase angle of the grid voltage and allows an easy computational time-delay compensation. In addition, a comparison of different control approaches to manage the MMC under unbalanced grid conditions is also presented, and advantages and disadvantages of these approaches are discussed in terms of capacitor voltage ripple, balancing performance, and negative-sequence current injection. The 401-level MMC of the INELFE project is considered to validate and test the proposed control schemes.

The paper is organized as follows. Sections II and III introduce the MMC model and the control of the converter currents, respectively. The strategy to balance the arm energies and the different approaches to control the MMC under unbalanced grid conditions are described in Section IV. In Section V, a thorough evaluation of the proposed and the conventional energy-based control schemes is presented. Finally, conclusions are drawn in Section VI.

II. MMC Model

Applying the Kirchhoff's laws to the electrical circuit of Fig. 1, the dynamic equations of the MMC currents can be written in the $o\alpha\beta$ stationary reference frame as follows (see [38] and [39]):

$$L_t \dot{\mathbf{i}}_g^{\alpha\beta} = -R_t \mathbf{i}_g^{\alpha\beta} + \mathbf{v}_g^{\alpha\beta} - \mathbf{v}_{\rm dif}^{\alpha\beta} \tag{1}$$

$$L_s \dot{\mathbf{i}}_{\rm cir}^{\alpha\beta} = -R_s \mathbf{i}_{\rm cir}^{\alpha\beta} + \mathbf{v}_{\rm sum}^{\alpha\beta} \tag{2}$$

$$^2/_3 L_s \dot{i}_{\rm dc} = -^2/_3 R_s i_{\rm dc} + \sqrt{2} v_{\rm sum}^o - v_{\rm dc} \tag{3}$$

where $\mathbf{i}_g^{\alpha\beta} = [\, i_g^\alpha \;\; i_g^\beta \,]^T$, $\mathbf{i}_{\rm cir}^{\alpha\beta} = [\, i_{\rm cir}^\alpha \;\; i_{\rm cir}^\beta \,]^T$, and $i_{\rm dc}$ are the ac-side current, the circulating current between converter phases, and the dc-side current, respectively; the following Clarke transformation is used to convert the variables from the abc reference frame to the $o\alpha\beta$ reference frame

$$\begin{bmatrix} x^o \\ x^\alpha \\ x^\beta \end{bmatrix} = \frac{2}{3} \begin{bmatrix} \frac{1}{\sqrt{2}} & \frac{1}{\sqrt{2}} & \frac{1}{\sqrt{2}} \\ 1 & -\frac{1}{2} & -\frac{1}{2} \\ 0 & -\frac{\sqrt{3}}{2} & \frac{\sqrt{3}}{2} \end{bmatrix} \begin{bmatrix} x^a \\ x^b \\ x^c \end{bmatrix}. \tag{4}$$

The superscripts o, α, and β stand for the zero, α-axis, and β-axis components. The parameters $R_t = R_e + {}^1/_2 R_s$ and $L_t = L_e + {}^1/_2 L_s$ are defined, as well as the auxiliary voltages

$$\mathbf{v}_{\rm sum} = \frac{\mathbf{v}_n + \mathbf{v}_p}{2}, \quad \mathbf{v}_{\rm dif} = \frac{\mathbf{v}_n - \mathbf{v}_p}{2} \tag{5}$$

where $\mathbf{v}_p$, $\mathbf{v}_n$, and $\mathbf{v}_g$ are the voltage vectors of the positive arms, negative arms, and ac grid, respectively. The rest of the variables and parameters are shown in Fig. 1.

The arm currents can be written as

$$i_p^z = \frac{i_{\rm dc}}{3} + \frac{i_g^z}{2} + i_{\rm cir}^z \tag{6}$$

$$i_n^z = \frac{i_{\rm dc}}{3} - \frac{i_g^z}{2} + i_{\rm cir}^z \tag{7}$$

where the subscript $z \in \{a, b, c\}$ represents a phase of the converter, and subscripts p and n indicate the positive and the negative terminal (see more details of the MMC modeling in [39] and [40]).

The dynamic equations of the SM capacitor voltages are

$$C^{\rm SM} \dot{v}_{Cp}^{{\rm SM}jz} = -\frac{v_{Cp}^{{\rm SM}jz}}{R^{\rm SM}} - s_p^{jz} i_p^z \tag{8}$$

$$C^{\rm SM} \dot{v}_{Cn}^{{\rm SM}jz} = -\frac{v_{Cn}^{{\rm SM}jz}}{R^{\rm SM}} - s_n^{jz} i_n^z \tag{9}$$

where s^j is 1 or 0 depending on the state (ON or OFF) of the corresponding IGBT (see Fig. 1), and the subscript $j \in \{1, \ldots, N\}$ represents the SM number in each arm. The sum of all capacitor

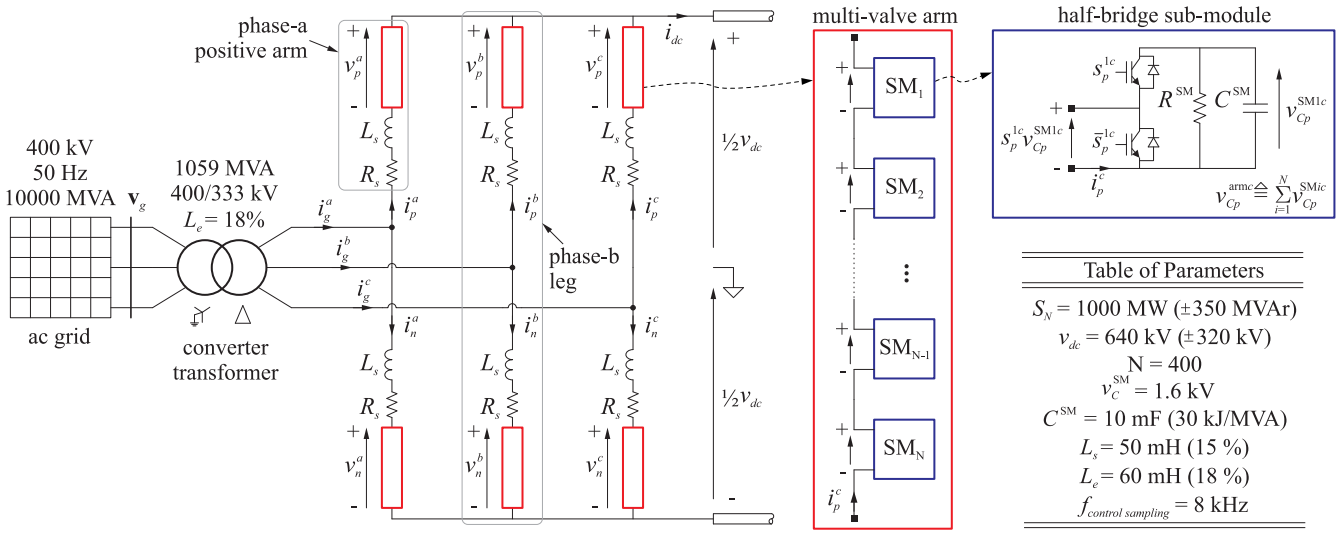

Fig. 1. Topology and parameters of the MMC.

voltages in one arm will be denoted by

$$v_{C\{p/n\}}^{\mathrm{arm}z} = \sum_{i=1}^{N} v_{C\{p/n\}}^{\mathrm{SM}iz}. \tag{10}$$

III. Control of the MMC Currents

The dynamic (1)–(3) can be written in a state-space representation of the general form $\dot{\mathbf{x}} = \mathbf{A}\mathbf{x} + \mathbf{B}\mathbf{u}$. This system in the continuous-time domain is digitized by using the zero-order hold discretization and represented in the discrete-time domain by $\mathbf{x}_{k+1} = \mathbf{G}\mathbf{x}_k + \mathbf{H}\mathbf{u}_k$, where the matrices of the discrete system are calculated as $\mathbf{G} = e^{\mathbf{A}T_s}$ and $\mathbf{H} = \int_0^{T_s} e^{\mathbf{A}\tau}\, d\tau \mathbf{B}$, being T_s the control sampling time [41]. Therefore, applying the above discretization to the continuous-time equations (1)–(3), the following discrete state-space representation is obtained

$$\mathbf{i}_{g(k+1)}^{\alpha\beta} = \mathbf{G}_t \mathbf{i}_{gk}^{\alpha\beta} + \mathbf{H}_t \mathbf{v}_{\mathrm{dif}k}^{\alpha\beta} - \mathbf{H}_t \mathbf{v}_{gk}^{\alpha\beta} \tag{11}$$

$$\mathbf{i}_{\mathrm{cir(k+1)}}^{\alpha\beta} = \mathbf{G}_s \mathbf{i}_{\mathrm{cir}k}^{\alpha\beta} + \mathbf{H}_s \mathbf{v}_{\mathrm{sum}k}^{\alpha\beta} \tag{12}$$

$$i_{\mathrm{dc(k+1)}} = G_{\mathrm{dc}} i_{\mathrm{dc}k} + H_{\mathrm{dc}} v_{\mathrm{sum}k}^{o} - {}^{1}\!/\!_{\sqrt{2}} H_{\mathrm{dc}} v_{\mathrm{dc}k}. \tag{13}$$

The currents $\mathbf{i}_g^{\alpha\beta}$, $\mathbf{i}_{\mathrm{cir}}^{\alpha\beta}$, and i_{dc} can be independently controlled by using the voltages $\mathbf{v}_{\mathrm{dif}}^{\alpha\beta}$, $\mathbf{v}_{\mathrm{sum}}^{\alpha\beta}$, and v_{sum}^{o}, respectively. Their controllers are designed using the decoupled current models (11)–(13); proportional-integral-resonant (PIR) control blocks are considered to track both dc and ac reference signals. The double-line frequency (2ω) components in both the circulating and the dc-side currents are eliminated by adding a proportional-resonant (PR) control block with 2ω resonance to their control loops. The control parameters are tuned using the optimal linear-quadratic method [42]. This approach of using PR controls in the stationary reference frame allows to control all the sequence components of the converter currents (i.e., zero, negative, and positive) without steady-state error. It does not require a grid phase tracking method, and it only uses a frequency-locked loop to adjust the resonance frequency [43]. The control model is also extended with an auxiliary variable $\mathbf{w}$ which goes one-sample time behind the control input (e.g., $\mathbf{v}_{dif\,k} = \mathbf{w}_{\mathrm{dif}(k-1)}$). In this way, the controller considers the computational time delay, improving the tracking performance, and having a faster transient response.

Once the duty cycles are computed from the controller, the nearest level control (NLC) modulation is used to obtain the IGBT gate signals. This staircase-type modulation is preferred for high-voltage and high-power applications (i.e., MMCs with high number of SMs) over other techniques based on pulse-width modulation, selective harmonic elimination, and nearest vector control, because it allows lower switching losses, lesser computational effort, and a simpler implementation [5]–[7]. A block diagram of the whole MMC control strategy is shown in Fig. 2 and further described in the next section.

IV. Strategy to Balance the Arm Energies

The energy-based control scheme controls and balances the SM capacitor voltages in two stages. In the first one (intra-arm balancing), the capacitor voltages inside each arm are equally distributed using a sorting algorithm with RSF modulation [44]. In the second stage (inter-arm balancing), outer control loops in cascade with the current controllers perform three tasks: the total energy control, the horizontal, and vertical energy balancing. This paper is mainly focused on this second stage.

The total energy control regulates the energy stored in all the converter capacitors (i.e., the sum of the six arm energies). The total stored energy is affected by the difference between the ac-side active power and the dc-side power. The horizontal energy balancing (or inter-leg energy balancing) equalizes the sum of the positive and negative arm energies of the three phase legs (i.e., it regulates the energy stored in the capacitors of each leg). The vertical energy balancing (or intra-leg energy balancing) nullifies the energy difference between the positive and the negative arm of each leg. These balancing and energy

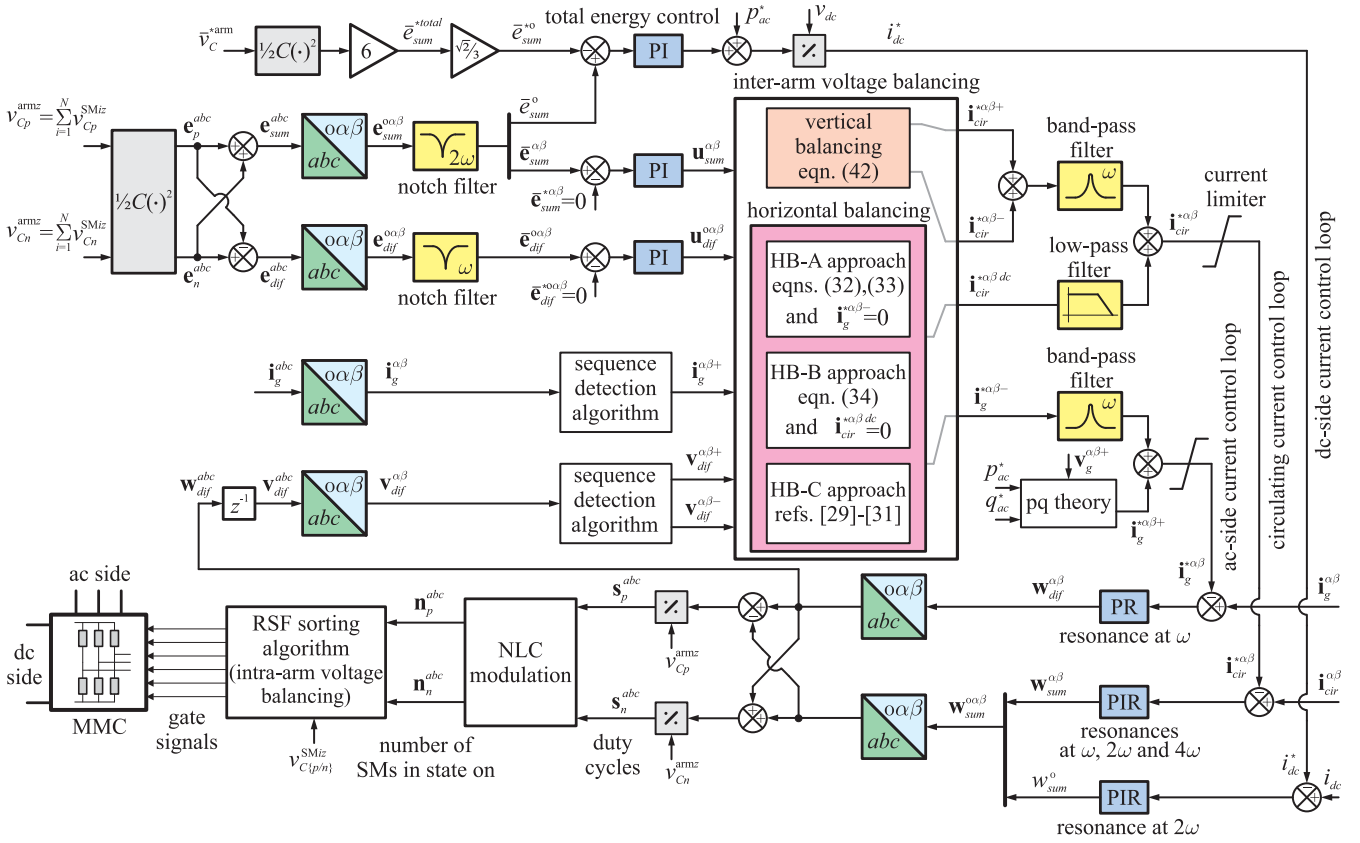

Fig. 2. Block diagram of the MMC control strategy including both voltage balancing and current control loops.

control tasks will be described in the following sections and extended to unbalanced ac grid conditions.

A. Arm Energies Under Unbalanced Grid Conditions

Considering (5)–(7) and neglecting resistive losses, the positive and negative arm powers $p_p^z = v_p^z i_p^z$ and $p_n^z = v_n^z i_n^z$ can be written as

$$\dot{e}_p^z = p_p^z = (v_{\rm sum}^z - v_{\rm dif}^z)\left(\frac{i_{\rm dc}}{3} + \frac{i_g^z}{2} + i_{\rm cir}^z\right) \quad (14)$$

$$\dot{e}_n^z = p_n^z = (v_{\rm sum}^z + v_{\rm dif}^z)\left(\frac{i_{\rm dc}}{3} - \frac{i_g^z}{2} + i_{\rm cir}^z\right) \quad (15)$$

where $\dot{e}_p^z$ and $\dot{e}_n^z$ are the time derivative of the arm energies. It can be seen that these energies are disturbed by the product of various voltage and current signals which have (under unbalanced grid conditions) zero-, negative-, and positive-sequence components together with a dc component. In the following, because the star/delta transformer blocks the zero-sequence currents [34], these zero-sequence terms are not considered.

Let us first calculate the power between a three-phase voltage signal and a three-phase current signal. Consider, for example, the a-phase of these generic signals, as follows:

$$v^a = V^+ \sin\left(\omega t + \theta^+\right) + V^- \sin\left(-\omega t + \theta^-\right) + v_{\rm dc} \quad (16)$$

$$i^a = I^+ \sin\left(\omega t + \varphi^+\right) + I^- \sin\left(-\omega t + \varphi^-\right) + i_{\rm dc}. \quad (17)$$

The superscripts $^+$ and $^-$ stand for the positive- and the negative-sequence components, and ω is the fundamental frequency. The magnitude and phase of the voltage (current) are represented by V and θ (I and φ), respectively, whereas $v_{\rm dc}$ ($i_{\rm dc}$) is its dc component. The resulting a-phase power $p^a = v^a i^a$ has several terms [see (18) shown at the bottom of the page]. The first five terms in (18) are non-alternating powers (i.e., they have a non-null mean value). Note that if these power terms are not compensated in (14) and (15), the mean value of the arm energies (in the following denoted by the symbol $\bar{e}$) can either rise or fall beyond an acceptable value. Moreover, some of these non-alternating powers depend on the negative-sequence components of the voltage and current signals. Consequently,

$$\begin{aligned} 2\dot{e}^a = \; & 2p^a = 2v_{\rm dc}i_{\rm dc} + V^+I^+\cos\left(\varphi^+ - \theta^+\right) + V^-I^-\cos\left(\varphi^- - \theta^-\right) - V^-I^+\cos\left(\varphi^+ + \theta^-\right) - V^+I^-\cos\left(\varphi^- + \theta^+\right) + V^-I^+ \\ & \times \cos\left(2\omega t + \varphi^+ - \theta^-\right) + V^+I^-\cos\left(\varphi^- - \theta^+ - 2\omega t\right) - V^+I^+\cos\left(2\omega t + \varphi^+ + \theta^+\right) - V^-I^-\cos\left(\varphi^- + \theta^- - 2\omega t\right) \\ & + 2v_{\rm dc}I^+\sin\left(\omega t + \varphi^+\right) + 2V^+i_{\rm dc}\sin\left(\omega t + \theta^+\right) + 2V^-i_{\rm dc}\sin\left(-\omega t + \theta^-\right) + 2v_{\rm dc}I^-\sin\left(-\omega t + \varphi^-\right) \end{aligned} \quad (18)$$

to achieve a precise control of the MMC, the negative-sequence components have to be considered not only when the current controller is designed, but also when the energy balancing is performed. The last eight terms in (18) are alternating powers which introduce ripples with frequencies ω and 2ω in the arm energies, but they do not deviate the energy mean value.

To analyze the horizontal and vertical energy balancing, it is useful to define the sum and difference between the arm energies in each phase of the converter; that is, $e^z_{\rm sum} = e^z_p + e^z_n$ and $e^z_{\rm dif} = e^z_p - e^z_n$. From (14) and (15), the dynamic equation of the sum and difference energies can be written using a vector notation in the abc stationary reference frame as follows:

$$\dot{\mathbf{e}}^{\rm abc}_{\rm sum} = \frac{2}{3}\mathbf{v}^{\rm abc}_{\rm sum} i_{\rm dc} - \mathbf{v}^{\rm abc}_{\rm dif} \circ \mathbf{i}^{\rm abc}_g + 2\mathbf{v}^{\rm abc}_{\rm sum} \circ \mathbf{i}^{\rm abc}_{\rm cir} \tag{19}$$

$$\dot{\mathbf{e}}^{\rm abc}_{\rm dif} = -\frac{2}{3}\mathbf{v}^{\rm abc}_{\rm dif} i_{\rm dc} + \mathbf{v}^{\rm abc}_{\rm sum} \circ \mathbf{i}^{\rm abc}_g - 2\mathbf{v}^{\rm abc}_{\rm dif} \circ \mathbf{i}^{\rm abc}_{\rm cir} \tag{20}$$

where $\circ$ stands for the element-by-element multiplication.

The voltage $\mathbf{v}_{\rm dif}$ and current $\mathbf{i}_g$ can have positive- and negative-sequence components. When the grid voltage is unbalanced (e.g., when $\mathbf{v}_g^- \neq 0$), the controller has to add a negative-sequence component to the voltage $\mathbf{v}_{\rm dif}$ to regulate the negative-sequence current $\mathbf{i}_g^-$. In a general case, the current $\mathbf{i}_g^-$ can be controlled to either a null or a non-null value depending on the criterion to inject negative-sequence current into the ac grid under unbalanced grid conditions [45]. This issue will be discussed below.

B. Total Energy Control and Horizontal Energy Balancing

In this section, three approaches are presented to control and equalize the energies $e^z_{\rm sum}$, thus achieving the total energy control and horizontal balancing. Transforming (19) to the $o\alpha\beta$ reference frame and proceeding as in (18), the mean value of the energy vector $\dot{\mathbf{e}}^{o\alpha\beta}_{\rm sum}$ has the following components:

$$\begin{aligned}\dot{\bar{e}}^{o}_{\rm sum} =\ & \frac{2\sqrt{2}}{3} v^{\rm dc}_{\rm sum} i_{\rm dc} - \frac{1}{\sqrt{2}} V^+_{\rm dif} I^+_g \cos\left(\varphi^+_g - \theta^+_{\rm dif}\right) \\ & - \frac{1}{\sqrt{2}} V^-_{\rm dif} I^-_g \cos\left(\varphi^-_g - \theta^-_{\rm dif}\right) \end{aligned} \tag{21}$$

$$\begin{aligned}\dot{\bar{e}}^{\alpha}_{\rm sum} =\ & 2v^{\rm dc}_{\rm sum} i^{\alpha\,{\rm dc}}_{\rm cir} + \frac{1}{2} V^+_{\rm dif} I^-_g \cos\left(\varphi^-_g + \theta^+_{\rm dif}\right) \\ & + \frac{1}{2} V^-_{\rm dif} I^+_g \cos\left(\varphi^+_g + \theta^-_{\rm dif}\right) \end{aligned} \tag{22}$$

$$\begin{aligned}\dot{\bar{e}}^{\beta}_{\rm sum} =\ & 2v^{\rm dc}_{\rm sum} i^{\beta\,{\rm dc}}_{\rm cir} + \frac{1}{2} V^+_{\rm dif} I^-_g \sin\left(\varphi^-_g + \theta^+_{\rm dif}\right) \\ & + \frac{1}{2} V^-_{\rm dif} I^+_g \sin\left(\varphi^+_g + \theta^-_{\rm dif}\right). \end{aligned} \tag{23}$$

Because the control is focused on regulating the mean value of the energies, only the non-alternating power terms are included on the right-side of (21)–(23). It is observed there that certain converter currents can be used to control the energy components $\bar{e}_{\rm sum}$. To obtain the references of these currents in the $o\alpha\beta$ reference frame, the current and voltage vectors are converted from Polar to Cartesian coordinates. A vector $\mathbf{x}$ can be represented by its magnitude X and phase ϕ, or by its components x^α and x^β as follows:

$$\mathbf{x}^\pm = X^\pm e^{j(\pm\omega t + \phi^\pm)} = x^{\beta\pm} + j x^{\alpha\pm}. \tag{24}$$

Applying (24) to the voltage vector $\mathbf{v}_{\rm dif}$ and current vector $\mathbf{i}_g$, the expressions for their positive- and negative-sequence components are given by

$$v^{\alpha\pm}_{\rm dif} = V^\pm_{\rm dif} \sin\left(\pm\omega t + \theta^\pm_{\rm dif}\right) \tag{25}$$

$$v^{\beta\pm}_{\rm dif} = V^\pm_{\rm dif} \cos\left(\pm\omega t + \theta^\pm_{\rm dif}\right) \tag{26}$$

$$i^{\alpha\pm}_g = I^\pm_g \sin\left(\pm\omega t + \varphi^\pm_g\right) \tag{27}$$

$$i^{\beta\pm}_g = I^\pm_g \cos\left(\pm\omega t + \varphi^\pm_g\right). \tag{28}$$

Using the relations (25)–(28) in (21)–(23), and after some algebraic manipulation, it results

$$\begin{aligned}\dot{\bar{e}}^{o}_{\rm sum} =\ & \frac{2\sqrt{2} v^{\rm dc}_{\rm sum} i_{\rm dc}}{3} - \frac{1}{\sqrt{2}}\left(v^{\alpha+}_{\rm dif} i^{\alpha+}_g + v^{\beta+}_{\rm dif} i^{\beta+}_g\right) \\ & - \frac{1}{\sqrt{2}}\left(v^{\alpha-}_{\rm dif} i^{\alpha-}_g + v^{\beta-}_{\rm dif} i^{\beta-}_g\right) \triangleq u^o_{\rm sum} \end{aligned} \tag{29}$$

$$\begin{aligned}\dot{\bar{e}}^{\alpha}_{\rm sum} =\ & 2v^{\rm dc}_{\rm sum} i^{\alpha\,dc}_{\rm cir} - \frac{1}{2}\left(v^{\alpha-}_{\rm dif} i^{\alpha+}_g + v^{\alpha+}_{\rm dif} i^{\alpha-}_g\right) \\ & + \frac{1}{2}\left(v^{\beta-}_{\rm dif} i^{\beta+}_g + v^{\beta+}_{\rm dif} i^{\beta-}_g\right) \triangleq u^\alpha_{\rm sum} \end{aligned} \tag{30}$$

$$\begin{aligned}\dot{\bar{e}}^{\beta}_{\rm sum} =\ & 2v^{\rm dc}_{\rm sum} i^{\beta\,dc}_{\rm cir} + \frac{1}{2}\left(v^{\alpha+}_{\rm dif} i^{\beta-}_g + v^{\beta+}_{\rm dif} i^{\alpha-}_g\right) \\ & + \frac{1}{2}\left(v^{\alpha-}_{\rm dif} i^{\beta+}_g + v^{\beta-}_{\rm dif} i^{\alpha+}_g\right) \triangleq u^\beta_{\rm sum}. \end{aligned} \tag{31}$$

The energy $\bar{e}^o_{\rm sum}$, proportional to the total stored energy, can be controlled (total energy control) by using either the dc power $p_{\rm dc} = v^{\rm dc}_{\rm sum} i_{\rm dc}$ or the positive-sequence active power $p^+_{ac} = v^{\alpha+}_{\rm dif} i^{\alpha+}_g + v^{\beta+}_{\rm dif} i^{\beta+}_g$ [see (29)]. This will depend on the MMC operating mode [16], [37]. On the other hand, the energies $\bar{e}^\alpha_{\rm sum}$ and $\bar{e}^\beta_{\rm sum}$ can be nullified (horizontal balancing) by using either the dc components of the circulating currents $i^{\alpha\,dc}_{\rm cir}$ and $i^{\beta\,dc}_{\rm cir}$ (called HB-A approach) or the fundamental-frequency negative-sequence currents $i^{\alpha-}_g$ and $i^{\beta-}_g$ (HB-B approach) [see (30) and (31)]. The components of the positive-sequence current $\mathbf{i}^+_g$ are not considered to accomplish this balancing because they will be used to control the active and reactive powers injected into the ac grid.

Steps or changes in voltages or currents of the MMC disturb the energies $\bar{e}_{\rm sum}$. By defining the auxiliary control inputs $u^o_{\rm sum}$, $u^\alpha_{\rm sum}$, and $u^\beta_{\rm sum}$ [see (29)–(31)], all the non-alternating power terms (disturbances) are compensated in a feed-forward manner. Then, after this control input transformation, a PI-based feedback control loop is designed to regulate $\bar{e}_{\rm sum}$ using the resulting first-order system $\dot{\bar{e}}_{\rm sum} = u_{\rm sum}$.

The current references to perform the horizontal balancing are obtained from (30) and (31). For the HB-A approach, these

references are given by

$$i_{\rm cir}^{\star\alpha\,{\rm dc}} = \frac{\overbrace{2u_{\rm sum}^{\alpha}}^{\text{feedback term}} + \overbrace{v_{\rm dif}^{\alpha-} i_g^{\alpha+} - v_{\rm dif}^{\beta-} i_g^{\beta+}}^{\text{feed-forward term}}}{4v_{\rm sum}^{\rm dc}} \tag{32}$$

$$i_{\rm cir}^{\star\beta\,{\rm dc}} = \frac{2u_{\rm sum}^{\beta} - v_{\rm dif}^{\alpha-} i_g^{\beta+} - v_{\rm dif}^{\beta-} i_g^{\alpha+}}{4v_{\rm sum}^{\rm dc}} \tag{33}$$

where the feedback and feed-forward terms have been indicated, and the superscript * stands for a reference value. For this approach, the negative-sequence currents injected into the ac grid are set to zero (i.e., $i_g^{\star\alpha-} = 0$ and $i_g^{\star\beta-} = 0$). The auxiliary control inputs $u_{\rm sum}^{\alpha}$ and $u_{\rm sum}^{\beta}$ are computed from the feedback control loops measuring the energy deviations, whereas the feed-forward terms consider the negative-sequence components to quickly reject the disturbance.

On the other hand, for the HB-B approach, the current references are obtained from (30) and (31) as

$$\begin{bmatrix} i_g^{\star\alpha-} \\ i_g^{\star\beta-} \end{bmatrix} = \begin{bmatrix} -v_{\rm dif}^{\alpha+} & v_{\rm dif}^{\beta+} \\ v_{\rm dif}^{\beta+} & v_{\rm dif}^{\alpha+} \end{bmatrix}^{-1} \begin{bmatrix} 2u_{\rm sum}^{\alpha} + v_{\rm dif}^{\alpha-} i_g^{\alpha+} - v_{\rm dif}^{\beta-} i_g^{\beta+} \\ 2u_{\rm sum}^{\beta} - v_{\rm dif}^{\alpha-} i_g^{\beta+} - v_{\rm dif}^{\beta-} i_g^{\alpha+} \end{bmatrix} \tag{34}$$

and the dc components of the circulating currents are set to zero (i.e., $i_{\rm cir}^{\star\alpha\,dc} = 0$ and $i_{\rm cir}^{\star\beta\,dc} = 0$).

Finally, the authors in [29]–[31] and [46] eliminate the 2ω ripple (appearing under unbalanced grid conditions) from the total stored energy of the MMC using the negative-sequence current $\mathbf{i}_g^-$, in the same way that it was previously proposed for traditional VSCs [27], [28]. Details on how to calculate the required current reference $\mathbf{i}_g^{\star-}$ for this approach are given in [29] and [47]. In the following, this approach will be called HB-C. Advantages and disadvantages of the three approaches will be analyzed in Section V-A.

C. Vertical Energy Balancing

In this section, the energies $e_{\rm dif}^{z}$ are nullified to achieve the vertical balancing. Similarly to the way performed in the previous section, transforming (20) to the $o\alpha\beta$ reference frame, the mean value components of the energy vector $\dot{\mathbf{e}}_{\rm dif}^{o\alpha\beta}$ results in

$$\dot{\bar{e}}_{\rm dif}^{o} = -\sqrt{2}\left(V_{\rm dif}^{-} I_{\rm cir}^{-} \cos\left(\varphi_{\rm cir}^{-} - \theta_{\rm dif}^{-}\right) + V_{\rm dif}^{+} I_{\rm cir}^{+} \cos\left(\varphi_{\rm cir}^{+} - \theta_{\rm dif}^{+}\right)\right) \tag{35}$$

$$\dot{\bar{e}}_{\rm dif}^{\alpha} = V_{\rm dif}^{-} I_{\rm cir}^{+} \cos\left(\varphi_{\rm cir}^{+} + \theta_{\rm dif}^{-}\right) + V_{\rm dif}^{+} I_{\rm cir}^{-} \cos\left(\varphi_{\rm cir}^{-} + \theta_{\rm dif}^{+}\right) \tag{36}$$

$$\dot{\bar{e}}_{\rm dif}^{\beta} = V_{\rm dif}^{-} I_{\rm cir}^{+} \sin\left(\varphi_{\rm cir}^{+} + \theta_{\rm dif}^{-}\right) + V_{\rm dif}^{+} I_{\rm cir}^{-} \sin\left(\varphi_{\rm cir}^{-} + \theta_{\rm dif}^{+}\right) \tag{37}$$

then, (35)–(37) are converted to Cartesian coordinates, obtaining

$$\dot{\bar{e}}_{\rm dif}^{o} = -\sqrt{2}\left(v_{\rm dif}^{\alpha-} i_{\rm cir}^{\alpha-} + v_{\rm dif}^{\beta-} i_{\rm cir}^{\beta-} + v_{\rm dif}^{\alpha+} i_{\rm cir}^{\alpha+} + v_{\rm dif}^{\beta+} i_{\rm cir}^{\beta+}\right) \triangleq u_{\rm dif}^{o} \tag{38}$$

$$\dot{\bar{e}}_{\rm dif}^{\alpha} = v_{\rm dif}^{\beta-} i_{\rm cir}^{\beta+} - v_{\rm dif}^{\alpha-} i_{\rm cir}^{\alpha+} - v_{\rm dif}^{\alpha+} i_{\rm cir}^{\alpha-} + v_{\rm dif}^{\beta+} i_{\rm cir}^{\beta-} \triangleq u_{\rm dif}^{\alpha} \tag{39}$$

$$\dot{\bar{e}}_{\rm dif}^{\beta} = v_{\rm dif}^{\alpha-} i_{\rm cir}^{\beta+} + v_{\rm dif}^{\beta-} i_{\rm cir}^{\alpha+} + v_{\rm dif}^{\alpha+} i_{\rm cir}^{\beta-} + v_{\rm dif}^{\beta+} i_{\rm cir}^{\alpha-} \triangleq u_{\rm dif}^{\beta}. \tag{40}$$

The energies $\bar{e}_{\rm dif}$ can be controlled by using the fundamental-frequency positive- and negative-sequence components of the circulating current $i_{\rm cir}^{\alpha+}$, $i_{\rm cir}^{\beta+}$, $i_{\rm cir}^{\alpha-}$, and $i_{\rm cir}^{\beta-}$ [see (38)–(40)]. The auxiliary control inputs $u_{\rm dif}^{o}$, $u_{\rm dif}^{\alpha}$, and $u_{\rm dif}^{\beta}$ are chosen to compensate in a feed-forward manner the non-alternating powers in the dynamics of $\bar{e}_{\rm dif}^{o}$, $\bar{e}_{\rm dif}^{\alpha}$, and $\bar{e}_{\rm dif}^{\beta}$, respectively. Then, these auxiliary control inputs are obtained from feedback control loops designed using the system $\dot{\bar{e}}_{\rm dif} = u_{\rm dif}$. Because there are four circulating current components to be chosen and only three energies to be controlled, an additional constraint is introduced imposing that the current $\mathbf{i}_{\rm cir}^{+}$ is in-phase with the voltage $\mathbf{v}_{\rm dif}^{+}$ (i.e., minimizing the injected apparent power [16], [17]). This condition can be established by zeroing the reactive power

$$q_{\rm cir}^{+} = v_{\rm dif}^{\alpha+} i_{\rm cir}^{\beta+} - v_{\rm dif}^{\beta+} i_{\rm cir}^{\alpha+} = 0. \tag{41}$$

Finally, the circulating current references to perform the vertical balancing are obtained from (38)–(40) and (41) as follows:

$$\begin{bmatrix} i_{\rm cir}^{\star\alpha+} \\ i_{\rm cir}^{\star\beta+} \\ i_{\rm cir}^{\star\alpha-} \\ i_{\rm cir}^{\star\beta-} \end{bmatrix} = \begin{bmatrix} -v_{\rm dif}^{\alpha+} & -v_{\rm dif}^{\beta+} & -v_{\rm dif}^{\alpha-} & -v_{\rm dif}^{\beta-} \\ -v_{\rm dif}^{\alpha-} & v_{\rm dif}^{\beta-} & -v_{\rm dif}^{\alpha+} & v_{\rm dif}^{\beta+} \\ v_{\rm dif}^{\beta-} & v_{\rm dif}^{\alpha-} & v_{\rm dif}^{\beta+} & v_{\rm dif}^{\alpha+} \\ -v_{\rm dif}^{\beta+} & v_{\rm dif}^{\alpha+} & 0 & 0 \end{bmatrix}^{-1} \begin{bmatrix} \dfrac{u_{\rm dif}^{o}}{\sqrt{2}} \\ u_{\rm dif}^{\alpha} \\ u_{\rm dif}^{\beta} \\ 0 \end{bmatrix}. \tag{42}$$

These circulating current components are only transiently used to achieve the vertical balancing; then, they are nullified in steady state. The whole MMC control strategy is shown in Fig. 2.

Note that when the energy-balancing control does not consider the non-alternating disturbance powers generated by the negative-sequence components, they have to be handled only by the integral action of feedback control loop. On the other hand, by adding a feed-forward compensation, these disturbances can be quickly compensated before the feedback control measures the energy deviation.

V. Performance Testing

The 1000-MW MMC with 400 SMs per arm of the INELFE project [6] was considered to assess the performance of the presented control schemes (see converter topology and parameters in Fig. 1). The tests were performed using detailed models from the SimPowerSystems toolbox of MATLAB/SIMULINK.

A. Comparison Among Balancing Approaches

The test of Fig. 3 shows the converter behavior using the HB-A, HB-B, and HB-C approaches (first, second, and third column,

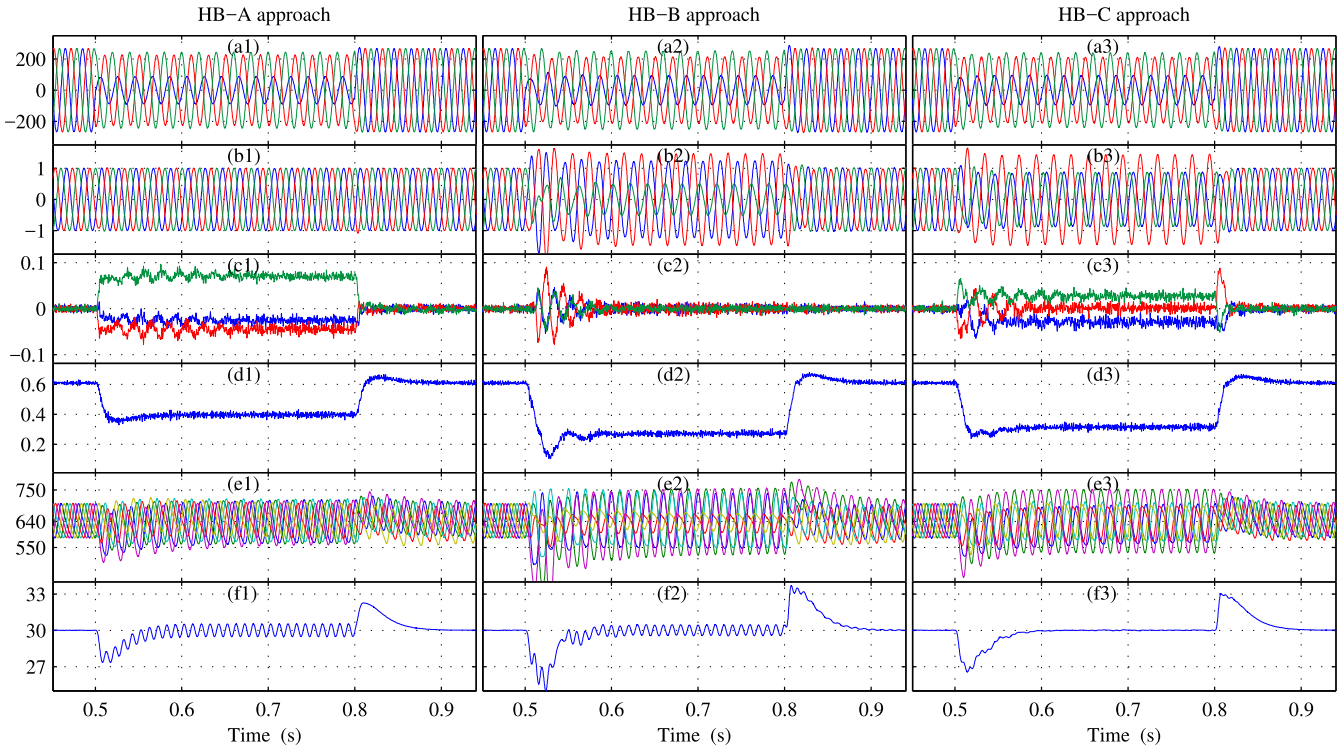

Fig. 3. Comparison among balancing approaches. (a) phase-to-ground ac voltage $\mathbf{v}_g$ [kV]. (b) ac-side current $\mathbf{i}_g$ [pu]. (c) Circulating current $\mathbf{i}_{\rm cir}$ [pu]. (d) dc-side current $i_{\rm dc}$ [pu]. (e) Sum of all capacitor voltages in each arm $v_{C\{p/n\}}^{{\rm arm}\,z}$ [kV]. (f) Total stored energy $e_{\rm sum}^{\rm total} \propto e_{\rm sum}^{o}$ [kJ/MVA].

respectively) during a single-phase-to-ground fault applied at 0.5 s and cleared at 0.8 s.

In the HB-A approach, the delivered grid currents are perfectly balanced at all times [i.e., $\mathbf{i}_g^- = 0$, see Fig. 3(b1)], and small dc components in the circulating currents (less than 0.1 per-unit) are injected to maintain the horizontal energy balancing under the unbalanced grid voltage condition [see Fig. 3(c1)]. This approach also shows an accurate control of the arm voltages at both the beginning and the end of the fault [see Fig. 3(e1)]. The HB-B approach has the advantage of eliminating all the circulating current components even under unbalanced grid voltages. However, to perform the horizontal balancing, it is necessary to inject a high negative-sequence current into the ac grid [see unbalanced grid currents in Fig. 3(b2)]. This additional current increases the total current of the arm, consequently increasing the converter losses, the IGBT stress, and the ripple in the capacitor voltages [compare Fig. 3(e2) to (e1)].

Finally, as expected for the HB-C approach, the total energy (sum of the six arm energies) has no 2ω ripple during the ac voltage imbalance [see Fig. 3(f3)]. However, similarly to the HB-B approach, this is achieved by injecting a relatively high negative-sequence current into the ac grid [see Fig. 3(b3)], with the aforementioned drawbacks in terms of IGBT current stress and capacitor voltage ripple. In the MMC, the ac output current passes through the SM capacitors; therefore, differently to what happens in the traditional VSC, the injected negative-sequence current increases the capacitor voltage ripple [compare Fig. 3(e3) to (e1)]. In the MMC, the energy is distributed among the six arms but, although the sum of the six arm energies is constant (without 2ω ripple), this does not mean that the energy of each individual arm is constant (i.e., that the arm voltages have a lower ripple). Therefore, the HB-C approach, originally proposed for traditional VSCs with concentrated or centralized capacitors at the dc bus, is not suitable for the MMC.

To summarize, the HB-A approach has more advantages, such as lower capacitor voltage ripple and balanced grid currents. In addition, in the three approaches, the 2ω components in both dc-side and circulating currents are eliminated during and after the asymmetrical fault [see Fig. 3(c) and (d)], thus reducing both the losses and the rated current of the arms, and also preventing that the ac-side imbalances affect the dc side.

B. Disturbance Rejection During Asymmetrical Faults

In this section, the previous unbalanced test was repeated in order to compare the proposed feedback/feed-forward control with conventional feedback controls. The transient response of the energy-based control using the HB-A approach (shown with black line in Fig. 4) was contrasted with the one of a conventional energy-based control (i.e., without considering the feed-forward terms). To improve the disturbance rejection capability of the conventional energy control, the bandwidth of its feedback control loop was increased by three, six, and ten times the bandwidth of the proposed control (red, blue, and green lines, respectively).

The vertical balancing performance, represented by the modulus (magnitude) of the energy vector $\bar{\mathbf{e}}_{\rm dif}^{\alpha\beta}$, is shown in Fig. 4(a). The control strategy with feed-forward terms quickly rejects the disturbance, thus allowing a better and faster energy balancing

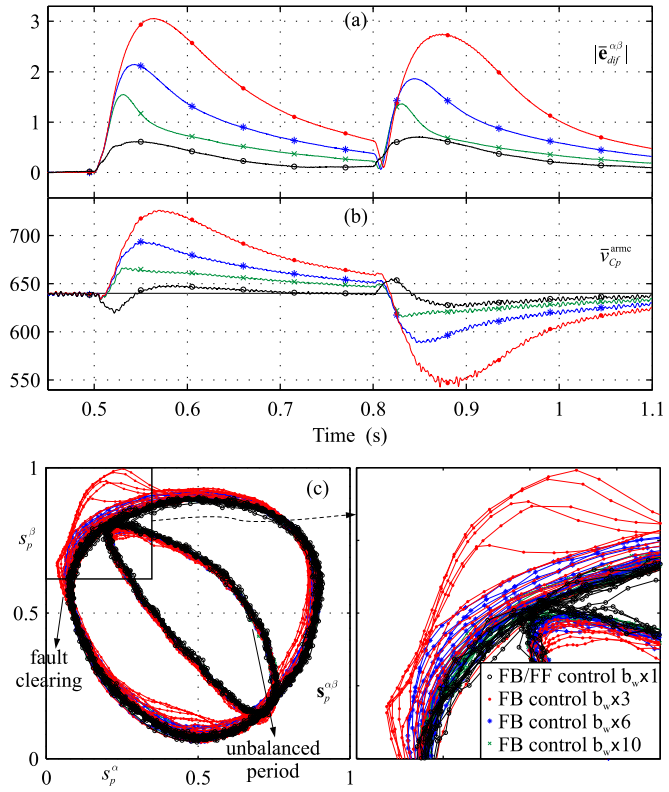

Fig. 4. Unbalanced test to compare the feedback/feed-forward control and three feedback controls with different bandwidths. (a) Magnitude of the energy vector $\bar{\mathbf{e}}_{\mathrm{dif}}^{\alpha\beta}$ [kJ/MVA]. (b) Mean value of the sum of all capacitor voltages in the phase-c positive arm $v_{Cp}^{\mathrm{arm}\,c}$ [kV]. (c) Duty cycle vector $\mathbf{s}_p^{\alpha\beta}$.

and even improving the performance of the conventional control with a ten times higher bandwidth (compare black line with circle markers to green line with cross markers). Similar conclusions can also be drawn by comparing the deviation of the voltage $\bar{v}_{Cp}^{\mathrm{arm}\,c}$ in Fig. 4(b).

When the proposed strategy synthesizes the arm voltages, due to its tighter capacitor voltage regulation, it is less prone to over-modulate in order to compensate the capacitor voltage drop [see duty cycle vector $\mathbf{s}_p^{\alpha\beta}$ in Fig. 4(c)]. On the other hand, the conventional control with lower disturbance rejection capability (i.e., larger dc voltage drop during a fault) is closer to reach the over-modulation range [see red lines in Fig. 4(c)].

C. Voltage Balancing and Changes in the Current Reference

Finally, a test under different converter operating modes was performed in order to assess the current control and voltage balancing tasks under balanced grid conditions (see Fig. 5). Initially, the MMC does not inject current into the ac grid (i.e., $\mathbf{i}_g^{\star} = 0$); then, at 0.4 s, a 50-ms ramp reference from zero to the rated current is given, and at 0.6 s the power flow is reversed with a 100-ms ramp from rectifier to inverter operation [see ac-side and dc-side current behavior in Fig. 5(a) and (b), respectively]. The reactive power reference is set to zero (unity power factor condition). At the beginning of the test, the arm energies (voltages) are set to different values [see Fig. 5(c)]. The horizontal and vertical balancing are shown in Fig. 5(d) and (e), where the sum and the difference energies $\bar{\mathbf{e}}_{\mathrm{sum}}^{\alpha\beta}$ and $\bar{\mathbf{e}}_{\mathrm{dif}}^{o\alpha\beta}$

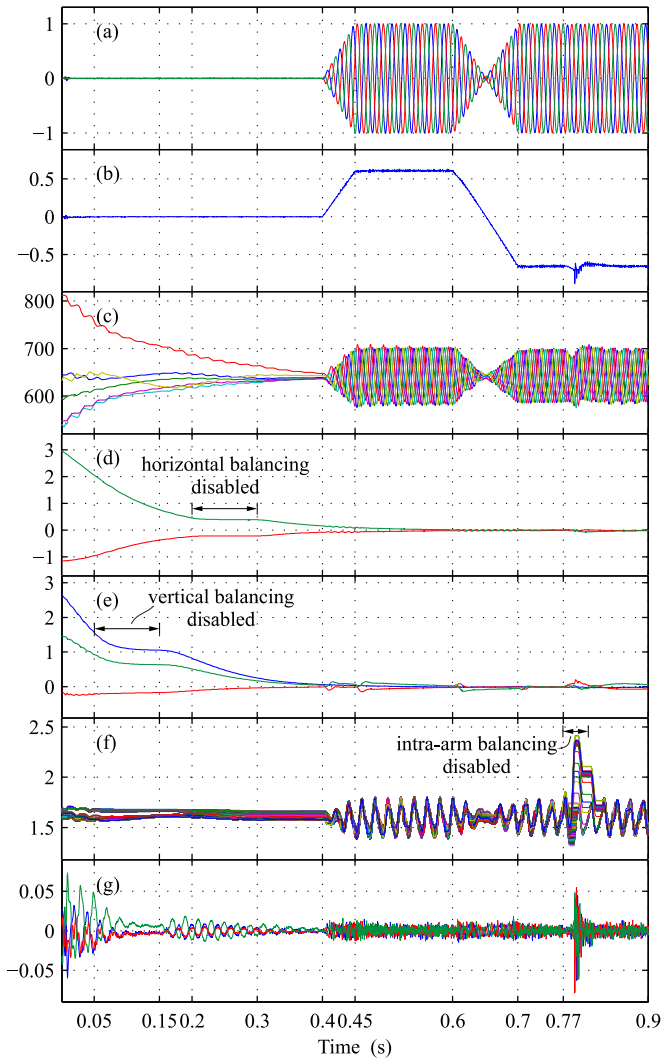

Fig. 5. Test under different operating conditions. (a) ac-side current $\mathbf{i}_g$ [pu]. (b) dc-side current i_{dc} [pu]. (c) Sum of all capacitor voltages in each arm $v_{C\{p/n\}}^{\mathrm{arm}\,z}$ [kV]. (d) Components of the sum energy vector (horizontal balancing) $\bar{\mathbf{e}}_{\mathrm{sum}}^{\alpha\beta}$ [kJ/MVA]. (e) Components of the difference energy vector (vertical balancing) $\bar{\mathbf{e}}_{\mathrm{dif}}^{o\alpha\beta}$ [kJ/MVA]. (f) All SM capacitor voltages of the phase-a positive arm $v_{Cp}^{\mathrm{SM}\,ia}$ [kV]. (g) Circulating current $\mathbf{i}_{\mathrm{cir}}$ [pu].

are presented. To clearly show the performance of the inter- and intra-arm balancing, their corresponding controls are disabled in some periods of time. For example, the vertical balancing is disabled between 0.05 and 0.15 s, the horizontal balancing between 0.2 and 0.3 s, and the intra-arm balancing between 0.77 and 0.79 s. It is observed that all capacitor voltages and arm energies are properly controlled for the different converter operating conditions. Fig. 5(g) shows how the fundamental frequency and dc components of the circulating current are transiently used to achieve the balancing tasks, and then nullified in steady state.

VI. Conclusion

A feedback/feed-forward control strategy was proposed to improve the voltage balancing of MMCs under unbalanced grid conditions. A detailed analysis of the power terms disturbing the inter-arm energy balancing was performed. Based on this

analysis, feed-forward compensations were designed for both horizontal and vertical balancing control loops. These compensation terms improved the transient response performance of the energy balancing under sudden grid voltage imbalances and asymmetrical faults (e.g., the most frequent single-phase-to-ground fault), thus enhancing the disturbance rejection and the fault ride-through capabilities of the converter. A comparison among the proposed and conventional energy-based control schemes was also performed, analyzing the capacitor voltage ripple, the IGBT stress, the balancing performance, and the negative-sequence current injection. Advantages and disadvantages of different approaches to achieve the voltage balancing were investigated, showing that the presented HB-A approach was the best option under unbalanced ac voltages. The design of discrete current controllers based on PR control blocks allowed a precise control of the ac-side, dc-side, and circulating currents as well as the elimination of their undesired 2ω components under unbalanced grid conditions. Several tests using the 401-level MMC of the INELFE project were performed to support and validate the proposed control strategy under both balanced and unbalanced grid conditions.

REFERENCES

[1] M. Perez, S. Bernet, J. Rodriguez, S. Kouro, and R. Lizana, "Circuit topologies, modeling, control schemes, and applications of modular multilevel converters," *IEEE Trans. Power Electron.*, vol. 30, no. 1, pp. 4–17, Jan. 2015.

[2] H. Saad *et al.*, "Modular multilevel converter models for electromagnetic transients," *IEEE Trans. Power Del.*, vol. 29, no. 3, pp. 1481–1489, Jun. 2014.

[3] A. Lesnicar and R. Marquardt, "An innovative modular multilevel converter topology suitable for a wide power range," in *Proc. IEEE Bologna Power Tech Conf.*, Jun. 2003, vol. 3, pp. 1–6.

[4] A. Alesina and M. Venturini, "Solid-state power conversion: A Fourier analysis approach to generalized transformer synthesis," *IEEE Trans. Circuits Syst.*, vol. 28, no. 4, pp. 319–330, Apr. 1981.

[5] P. M. Meshram and V. B. Borghate, "A simplified nearest level control (NLC) voltage balancing method for modular multilevel converter (MMC)," *IEEE Trans. Power Electron.*, vol. 30, no. 1, pp. 450–462, Jan. 2015.

[6] J. Peralta, H. Saad, S. Dennetiere, J. Mahseredjian, and S. Nguefeu, "Detailed and averaged models for a 401-level MMC-HVDC system," *IEEE Trans. Power Del.*, vol. 27, no. 3, pp. 1501–1508, Jul. 2012.

[7] S. Debnath, J. Qin, B. Bahrani, M. Saeedifard, and P. Barbosa, "Operation, control, and applications of the modular multilevel converter: A review," *IEEE Trans. Power Electron.*, vol. 30, no. 1, pp. 37–53, Jan. 2015.

[8] R. Darus, J. Pou, G. Konstantinou, S. Ceballos, R. Picas, and V. Agelidis, "A modified voltage balancing algorithm for the modular multilevel converter: Evaluation for staircase and phase-disposition PWM," *IEEE Trans. Power Electron.*, vol. 30, no. 8, pp. 4119–4127, Aug. 2015.

[9] Y. Li, E. A. Jones, and F. Wang, "The impact of voltage-balancing control on switching frequency of the modular multilevel converter," *IEEE Trans. Power Electron.*, vol. 31, no. 4, pp. 2829–2839, Apr. 2016.

[10] K. Ilves, L. Harnefors, S. Norrga, and H. P. Nee, "Predictive sorting algorithm for modular multilevel converters minimizing the spread in the submodule capacitor voltages," *IEEE Trans. Power Electron.*, vol. 30, no. 1, pp. 440–449, Jan. 2015.

[11] A. Antonopoulos, L. Angquist, and H.-P. Nee, "On dynamics and voltage control of the modular multilevel converter," in *Proc. Eur. Conf. Power Electron. Appl.*, Sep. 2009, pp. 1–10.

[12] P. Munch, D. Gorges, M. Izak, and S. Liu, "Integrated current control, energy control and energy balancing of modular multilevel converters," in *Proc. Annu. Conf. IEEE Ind. Electr. Soc.*, Nov. 2010, pp. 150–155.

[13] Y. Wan, S. Liu, and J. Jiang, "Generalised analytical methods and current-energy control design for modular multilevel cascade converter," *IET Power Electron.*, vol. 6, no. 3, pp. 495–504, Mar. 2013.

[14] G. Bergna *et al.*, "An energy-based controller for HVDC modular multilevel converter in decoupled double synchronous reference frame for voltage oscillation reduction," *IEEE Trans. Ind. Electron.*, vol. 60, no. 6, pp. 2360–2371, Jun. 2013.

[15] S. Cui, S. Kim, J.-J. Jung, and S.-K. Sul, "A comprehensive cell capacitor energy control strategy of a modular multilevel converter (MMC) without a stiff dc bus voltage source," in *Proc. Annu. IEEE Appl. Power Electr. Conf. Expo*, Mar. 2014, pp. 602–609.

[16] S. Fan, K. Zhang, J. Xiong, and Y. Xue, "An improved control system for modular multilevel converters with new modulation strategy and voltage balancing control," *IEEE Trans. Power Electron.*, vol. 30, no. 1, pp. 358–371, Jan. 2015.

[17] J. Kolb, F. Kammerer, M. Gommeringer, and M. Braun, "Cascaded control system of the modular multilevel converter for feeding variable-speed drives," *IEEE Trans. Power Electron.*, vol. 30, no. 1, pp. 349–357, Jan. 2015.

[18] Q. Xu, F. Ma, A. Luo, Y. Chen, and Z. He, "Hierarchical direct power control of modular multilevel converter for tundish heating," *IEEE Trans. Ind. Electron.*, 2016, to be published.

[19] F. Zhang, W. Li, and G. Joos, "A voltage-level-based model predictive control of modular multilevel converter," *IEEE Trans. Ind. Electron.*, vol. 63, no. 8, pp. 5301–5312, Aug. 2016.

[20] P. Liu, Y. Wang, W. Cong, and W. Lei, "Grouping-sorting-optimized model predictive control for modular multilevel converter with reduced computational load," *IEEE Trans. Power Electron.*, vol. 31, no. 3, pp. 1896–1907, Mar. 2016.

[21] G. Konstantinou, J. Pou, S. Ceballos, R. Picas, J. Zaragoza, and V. G. Agelidis, "Control of circulating currents in modular multilevel converters through redundant voltage levels," *IEEE Trans. Power Electron.*, vol. 31, no. 11, pp. 7761–7769, Nov. 2016.

[22] B. Bahrani, S. Debnath, and M. Saeedifard, "Circulating current suppression of the modular multilevel converter in a double-frequency rotating reference frame," *IEEE Trans. Power Electron.*, vol. 31, no. 1, pp. 783–792, Jan. 2016.

[23] A. Dekka, B. Wu, V. Yaramasu, and N. Zargari, "Model predictive control with common-mode voltage injection for modular multilevel converter," *IEEE Trans. Power Electron.*, 2016, to be published.

[24] M. Saeedifard and R. Iravani, "Dynamic performance of a modular multilevel back-to-back HVDC system," *IEEE Trans. Power Del.*, vol. 25, no. 4, pp. 2903–2912, Oct. 2010.

[25] Q. Tu, Z. Xu, Y. Chang, and L. Guan, "Suppressing dc voltage ripples of MMC-HVDC under unbalanced grid conditions," *IEEE Trans. Power Del.*, vol. 27, no. 3, pp. 1332–1338, Jul. 2012.

[26] X. Shi, Z. Wang, B. Liu, Y. Liu, L. Tolbert, and F. Wang, "Characteristic investigation and control of a modular multilevel converter-based HVDC system under single-line-to-ground fault conditions," *IEEE Trans. Power Electron.*, vol. 30, no. 1, pp. 408–421, Jan. 2015.

[27] M. Guan and Z. Xu, "Modeling and control of a modular multilevel converter-based HVDC system under unbalanced grid conditions," *IEEE Trans. Power Electron.*, vol. 27, no. 12, pp. 4858–4867, Dec. 2012.

[28] S. Li, X. Wang, Z. Yao, T. Li, and Z. Peng, "Circulating current suppressing strategy for MMC-HVDC based on nonideal proportional resonant controllers under unbalanced grid conditions," *IEEE Trans. Power Electron.*, vol. 30, no. 1, pp. 387–397, Jan. 2015.

[29] Y. Zhou, D. Jiang, J. Guo, P. Hu, and Y. Liang, "Analysis and control of modular multilevel converters under unbalanced conditions," *IEEE Trans. Power Del.*, vol. 28, no. 4, pp. 1986–1995, Oct. 2013.

[30] J.-W. Moon, C.-S. Kim, J.-W. Park, D.-W. Kang, and J.-M. Kim, "Circulating current control in MMC under the unbalanced voltage," *IEEE Trans. Power Del.*, vol. 28, no. 3, pp. 1952–1959, Jul. 2013.

[31] J.-W. Moon, J.-W. Park, D.-W. Kang, and J.-M. Kim, "A control method of HVDC-modular multilevel converter based on arm current under the unbalanced voltage condition," *IEEE Trans. Power Del.*, vol. 30, no. 2, pp. 529–536, Apr. 2015.

[32] M. Vasiladiotis, N. Cherix, and A. Rufer, "Impact of grid asymmetries on the operation and capacitive energy storage design of modular multilevel converters," *IEEE Trans. Ind. Electron.*, vol. 62, no. 11, pp. 6697–6707, Nov. 2015.

[33] Y. Liang, J. Liu, T. Zhang, and Q. Yang, "Arm current control strategy for MMC-HVDC under unbalanced conditions," *IEEE Trans. Power Del.*, 2016, to be published.

[34] S. Wenig, F. Rojas, K. Schonleber, M. Suriyah, and T. Leibfried, "Simulation framework for dc grid control and ACDC interaction studies based on modular multilevel converters," *IEEE Trans. Power Del.*, vol. 31, no. 2, pp. 780–788, Apr. 2016.

[35] J.-J. Jung, S. Cui, Y. Lee, and S.-K. Sul, "A cell capacitor energy balancing control of MMC-HVDC under the AC grid faults," in *Proc. Asia Int. Conf. Power Electron.*, Jun. 2015, pp. 1–8.
[36] S. Cui, H.-J. Lee, J.-J. Jung, Y. Lee, and S.-K. Sul, "A comprehensive AC side single line to ground fault ride through strategy of a modular multilevel converter for HVDC system," in *Proc. IEEE Energy Convers. Congr. Expo.*, Sep. 2015, pp. 5378–5385.
[37] D. Soto-Sanchez and T. Green, "Control of a modular multilevel converter-based HVDC transmission system," in *Proc. Eur. Conf. Power Electron. Appl.*, Aug. 2011, pp. 1–10.
[38] R. Lizana, C. Castillo, M. Perez, and J. Rodriguez, "Capacitor voltage balance of MMC converters in bidirectional power flow operation," in *Proc. Annu. Conf. IEEE Ind. Electr. Soc.*, Oct. 2012, pp. 4935–4940.
[39] J. Wang, R. Burgos, and D. Boroyevich, "Switching-cycle state-space modeling and control of the modular multilevel converter," *IEEE J. Emerg. Sel. Topics Power Electron.*, vol. 2, no. 4, pp. 1159–1170, Dec. 2014.
[40] G. Adam and B. Williams, "Half- and full-bridge modular multilevel converter models for simulations of full-scale HVDC links and multiterminal dc grids," *IEEE J. Emerg. Sel. Topics Power Electron.*, vol. 2, no. 4, pp. 1089–1108, Dec. 2014.
[41] K. Ogata, *Discrete-Time Control Systems*, 2nd ed. Englewood Cliffs, NJ, USA: Prentice-Hall, 1995.
[42] A. E. Leon and J. A. Solsona, "Performance improvement of full-converter wind turbines under distorted conditions," *IEEE Trans. Sustainable Energy*, vol. 4, no. 3, pp. 652–660, Jul. 2013.
[43] P. Rodriguez, A. Luna, R. Muñoz-Aguilar, I. Etxeberria-Otadui, R. Teodorescu, and F. Blaabjerg, "A stationary reference frame grid synchronization system for three-phase grid-connected power converters under adverse grid conditions," *IEEE Trans. Power Electron.*, vol. 27, no. 1, pp. 99–112, Jan. 2012.
[44] Q. Tu and Z. Xu, "Impact of sampling frequency on harmonic distortion for modular multilevel converter," *IEEE Trans. Power Del.*, vol. 26, no. 1, pp. 298–306, Jan. 2011.
[45] A. E. Leon, J. M. Mauricio, J. A. Solsona, and A. Gomez-Exposito, "Software sensor-based STATCOM control under unbalanced conditions," *IEEE Trans. Power Del.*, vol. 24, no. 3, pp. 1623–1632, Jul. 2009.
[46] J.-W. Moon, J.-S. Gwon, J.-W. Park, D.-W. Kang, and J.-M. Kim, "Model predictive control with a reduced number of considered states in a modular multilevel converter for HVDC system," *IEEE Trans. Power Del.*, vol. 30, no. 2, pp. 608–617, Apr. 2015.
[47] A. E. Leon, J. M. Mauricio, J. A. Solsona, and A. Gomez-Exposito, "Adaptive control strategy for VSC-based systems under unbalanced network conditions," *IEEE Trans. Smart Grid*, vol. 1, no. 3, pp. 311–319, Dec. 2010.

Andres E. Leon (S'05–M'13–SM'16) received the degree in electrical engineering from the Universidad Nacional del Comahue, Neuquén, Argentina, and the Ph.D. degree in control systems from the Universidad Nacional del Sur, Bahía Blanca, Argentina, in 2005 and 2011, respectively.

Since 2012, he has been a Researcher of the National Scientific and Technical Research Council. He is currently working at the Research Institute of Electrical Engineering "Alfredo Desages", Bahía Blanca, Argentina. He is an Associate Editor of the IEEE TRANSACTIONS ON SUSTAINABLE ENERGY. His research interests include power system control and wind energy conversion systems.

Santiago J. Amodeo received the B.S. degree in electrical engineering from the Universidad Nacional del Sur, Bahía Blanca, Argentina, in 2005.

He has been a Teaching Assistant and Postgraduate Student at the Department of Electrical and Computer Engineering, Universidad Nacional del Sur, Bahía Blanca, Argentina, since 2006. He is currently the Director of the ElectroAMSA Company. His main research interests include electrical machines and power electronics.